Journal of Chromatography B, 877 (2009) 1335–1343

Contents lists available at ScienceDirect

Journal of Chromatography B

journal homepage: www.elsevier.com/locate/chromb

Quantitative proteomic analysis of follicular lymphoma cells in response to rituximab☆

Kathryn L. Everton[a], David R. Abbott[a], David K. Crockett[b], Kojo S.J. Elenitoba-Johnson[c], Megan S. Lim[c,*]

[a] Department of Pathology, University of Utah School of Medicine, Salt Lake City, UT, United States
[b] ARUP Institute for Clinical and Experimental Pathology, Salt Lake City, UT, United States
[c] Department of Pathology, University of Michigan, Ann Arbor, MI, United States

ARTICLE INFO

Article history:
Available online 28 October 2008

Keywords:
Rituximab
Drug therapy
Protein interactions
MS/MS
In silico

ABSTRACT

Rituximab is a monoclonal antibody that targets the uniquely expressed B-cell CD20 receptor. Although recently approved for treatment of follicular lymphomas, the intracellular events that occur when rituximab binds to CD20 are largely unknown. Quantitative proteomic analysis of B-cell lymphoma-derived cells exposed to rituximab was performed. Differentially expressed proteins belonged to functional groups involved in migration, adhesion, calcium-induced signaling, ubiquitination, and components of the phosphoinositol and NF-κB pathways. Our studies reveal the proteomic consequences of rituximab treatment and provide novel insights into the mechanism of action of the drug in susceptible B-cell lymphoproliferative disorders.

1. Introduction

Rituximab is a human chimeric monoclonal antibody that targets the CD20 antigen uniquely expressed on B-cells. CD20 is a 35–37 kDa tetraspan membrane protein that is not expressed on hematopoietic stem cells, plasma cells or any other tissue in the body, making it an ideal target for the therapy of B-cell malignancies [1]. Rituximab is used in combination with other drugs (R-CHOP) in initial treatment and in the relapsed setting for a variety of B-cell non-Hodgkin lymphomas, including follicular lymphoma, diffuse large B-cell lymphoma and mantle cell lymphoma. Furthermore, investigations into the effectiveness of rituximab against a variety of B-cell related autoimmune disorders including multiple sclerosis, autoimmune hemolytic anemia, systemic lupus erythematosus, immune thrombocytopenic purpura and rheumatoid arthritis is currently underway [2].

Four major mechanisms have been proposed to account for the activity of rituximab in B-cell lymphoproliferative disorders: (1) apoptosis and proliferation inhibition via intracellular signaling, (2) increased sensitivity to other chemotherapeutic drugs, (3) complement-dependent cytotoxicity (CDC), and 4) antibody-dependent cellular cytotoxicity (ADCC) [3]. A combination of all four mechanisms has also been proposed as the mechanism of action. However, the intracellular events that occur in B-cells in response to rituximab are largely unknown.

We propose that comparison of protein expression in rituximab-treated lymphoma-derived cells with that of untreated cells will be useful in elucidating the intracellular mechanism(s) of rituximab action. Quantitative proteomic analysis is a direct way of looking at perturbations of normal cell activity due to drugs, cancer and a variety of other disease processes [4].

In this study, we carried out quantitative analysis of differential protein expression between B-cell lymphoma cells treated with rituximab and untreated (control) cells using the cleavable isotope-coded affinity tag (ICAT) strategy. Isotope-coded affinity tag analysis is useful because (1) peptides can be harvested from cells or tissues in any growth condition, (2) labeling is possible even in the presence of detergents or salts, (3) the complexity of the samples are reduced by isolating the cysteine-containing peptides, and (4) it is compatible with almost any method of fractionation to enrich for low abundance proteins [4].

Abbreviations: ADCC, antibody-dependent cellular cytotoxicity; amu, atomic mass units; B-NHL, B-cell non-Hodgkin's lymphoma; CDC, complement-dependent cytotoxicity; ICAT, isotope-coded affinity tag; LC, liquid chromatography; MS/MS, tandem mass spectrometry; SCX, strong cation exchange; GWAS, genome wide association study.

☆ This paper is part of the special issue "Quantitative analysis of biomarkers by LC–MS/MS", J. Cummings, R.D. Unwin and T. Veenstra (Guest Editors).

* Corresponding author at: University of Michigan, Department of Pathology, M5242 Medical Science I, 1301 Catherine St., Ann Arbor, MI 48109-0602, United States. Tel.: +1 734 936 1874; fax: +1 734 936 2756.
E-mail address: meganlim@umich.edu (M.S. Lim).

1570-0232/$ – see front matter © 2008 Elsevier B.V. All rights reserved.
doi:10.1016/j.jchromb.2008.10.036

Our quantitative analysis of differentially expressed proteins revealed the deregulation of proteins in several functional groups, including proteins involved in migration and adhesion, calcium-induced signaling, and components of the phosphoinositol and NF-κB signaling pathways. These results indicate broader cellular consequences of rituximab administration than speculated in previous studies.

2. Experimental

2.1. Cell culture

A CD20-positive B-cell non-Hodgkin's lymphoma (B-NHL)-derived cell line, SUDHL-4, was used. Cells were maintained at 37 °C with 5% CO_2 in RPMI 1640 medium (Novatech, Inc.) supplemented with 10% heat-inactivated fetal calf serum, and antibiotic mixture (Gibco-BRL).

2.2. Cell viability analysis

As indicated by the protocol provided by American Type Culture Collection (Manassa, VA), cells were diluted to 100,000 cells/mL and incubated with rituximab at varying concentrations (10, 20, and 50 μg/mL) or without the drug (media control) for several time points (24, 48, 72, and 96 h). Samples of 100 μL from treated and untreated cells were then added to 20 μL MTT (5 mg/mL) in a 96-well plate and incubated for 2 h. Cells were lysed with 100 μL lysis buffer. Absorbance was recorded at 570 nm.

2.3. Caspase-3 activity assay

Using the colorimetric CaspACE™ assay protocol (Promega Corp., Madison, WI), 2×10^6 cells (rituximab 10 μg/mL and untreated) were harvested and washed with cold PBS. Cells were resuspended in lysis buffer and lysed by freezing and thawing. Lysates were incubated on ice for 15 min, and then centrifuged at 15,000 rpm for 20 min. The supernatant was collected and caspase-3 activity was measured according to protocol, measuring final absorbance at 405 nm.

2.4. Cell cycle analysis

Flow cytometry was performed to analyze the proportions of cells in each phase of the cell cycle (G_1, S, G_2, M). We collected 1×10^6 cells, treated and untreated, using centrifugation at 2500 rpm for 10 min at 4 °C. The cells were resuspended in 500 μL cold PBS and 4.5 mL cold 200 proof ethanol. After incubation at 4 °C for 2 h, cells were stained with propidium iodide 50 μg/mL in PBS containing 200 U/mL of RNase and incubated for 30 min. The cells were analyzed by flow cytometry using Cell Quest (BD Biosciences) for data acquisition and analysis.

2.5. ICAT analysis

Equal amounts of protein (800 μg) from each sample (control and treated) were reduced with 2.5 mM Tris[2-carboxyethyl] phosphine (Pierce, Rockton, IL) for 30 min at 37 °C. ICAT labeling was carried out by mixing 10 units of light (control samples) or heavy (treated samples) cleavable ICAT (Applied Biosystems, Foster City, CA) with protein samples following manufacturer's instruction, and then samples were incubated for 90 min at 37 °C. Labeled proteins were mixed and then diluted 2.0-fold with 10 mM Tris, pH 8.5 before digestion with 20 μg modified trypsin (Promega, Madison, WI) overnight at 37 °C.

The peptide mixture was then acidified to pH 3.0 by adding trifluoroacetic acid before loading into the cation-exchange column. The three-dimensional liquid chromatographic separation of peptides was carried out as follows. Strong cation-exchange (SCX) chromatography using a 3.6 mm × 20 cm polysulfoethyl A column (Poly LC Inc., Columbia, MD) at a flow rate of 400 μL/min with 45 fractions collected (600 μL/fraction). A two-step linear buffer gradient was used: 5% buffer B and 95% buffer A to 25% buffer B and 75% buffer A for 50 min followed by 25% buffer B and 75% buffer A to 100% buffer B for 18 min (buffer A, 20 mM KH_2PO_4, 25% acetonitrile, pH 3.0; buffer B, 350 mM KCl in buffer A, pH 3.0). Using spectrometer readings as a guideline, the 45 SCX fractions were combined into 15 fractions and further purified by an ultralink monomeric avidin affinity cartridge (Applied Biosystems, Foster City, CA) to select for the cysteine-containing peptides (ICAT-labeled peptides). The eluted peptides were then dried and cleaved as per the manufacturer's instructions.

Digested peptides were injected by a Surveyor autosampler (Thermo, San Jose, CA), using an acetonitrile gradient (0–60% B in 120 min; A = 5% acetonitrile with 0.4% acetic acid and 0.005% HFBA) through a reverse phase column (75 μm i.d. fused silica packed in-house with 10 cm of 5 μm C18 particles) to elute the peptides at a flow rate of ~200 nL/min into an LCQ Deca XP ion trap mass spectrometer (Thermo). An electrospray voltage of 1.8 kV was used with the ion transfer tube temperature set to 200 °C. Peptide analysis was performed using data-dependent acquisition of one MS scan (600–2000 m/z) followed by MS/MS scans of ICAT peptide pairs triggered by the isotope tag mass difference of 9.0 atomic mass units (amu). Dynamic exclusion was set to a repeat count of 3, with the exclusion duration of 5 min.

2.6. Peptide searching and database analysis

The MS/MS acquired data were searched using the SEQUEST algorithm in Bioworks 3.1 SR1 (Thermo) against amino acid sequences in the International Protein Index (IPI) human protein database (v3.15, 9/21/07 download–55,041 entries) [5]. Protein search parameters included a precursor peptide mass tolerance of ±0.7 amu, and fragment mass tolerance of ±0.1 amu. Static modification of cysteine was set as 227.13 and differential modification of cysteine set as 9.0. The search was constrained to tryptic peptides with one missed enzyme cleavage allowed. The peptide matching criteria of a cross correlation score (X_{corr}) >1.8 for +1 peptides, >2.5 for +2 peptides, and >3.5 for +3 peptides, and a delta correlation score (ΔC_n) >0.100 was used as a threshold of acceptance.

The false positive error rate for protein identifications was estimated using the composite target/decoy database method [6]. Overall the predicted false positive rate for protein identification by LC–MS/MS was 11.4%. Protein quantification was performed using both ASAPRatio and Xpress which automatically calculates the relative abundance of light and heavy ICAT-labeled peptide as a ratio of light versus heavy [4,7].

The SEQUEST data (.dta) and output (.out) files were also analyzed using a second suite of tools; INTERACT and ProteinProphet (Institute for Systems Biology, Seattle, WA) [8,9]. Data analysis using INTERACT and ProteinProphet assesses the confidence of protein identification by best-fit distribution of probability scores specific to the data set, and reduced the risk of false positive protein identifications. We selected only proteins passing a threshold of less than 5% predicted error for inclusion in our final list. Finally, the tandem mass spectra for each of the identified proteins were verified by manual inspection to further diminish the likelihood of false identifications.

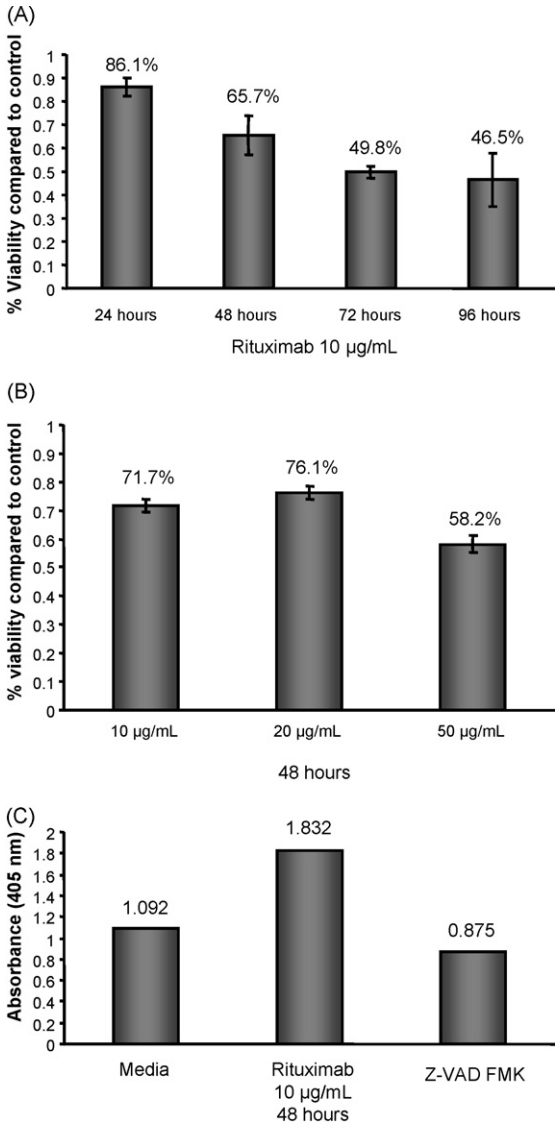

Fig. 1. The effect of rituximab on viability of SUDHL-4 cells was determined by MTT assay. (A) Rituximab (10 μg/mL) induced a time-course dependent decrease in cell viability of SUDHL-4 cells ($n = 3$). The percentage of cell viability is expressed relative to control cells that were exposed to media alone. The data represent the mean ± the standard error of the mean of triplicate measurements. (B) Increasing concentrations of rituximab did not have a significant effect on the viability of SUDHL-4 cells. Cells were exposed to varying concentrations (10, 20, and 50 μg/mL) of rituximab and MTT assay was performed at a 48 h time point. The data represent the mean ± the standard error of the mean of triplicate measurements. (C) Rituximab induced caspase-3 activity which was abrogated by the pan-caspase inhibitor Z-VAD FMK. Caspase-3 activity of SUDHL-4 cells exposed to rituximab (10 μg/mL for 48 h), media alone and the caspase inhibitor Z-VAD FMK was measured using a colorimetric assay ($n = 2$). The data represent the mean of two independent measurements.

2.7. Pathway analysis

Differentially expressed proteins were further analyzed using the Ingenuity Pathways Analysis bioinformatics software package (www.ingenuity.com). Protein accession numbers and corresponding ICAT expression values were saved into the Ingenuity Systems template.xls file. Files were submitted on-line for analysis and comparison to the Ingenuity gene/protein interaction knowledge base. Networks were subsequently merged for display and putative canonical pathways are represented in text boxes. The nodes represent proteins while the edges represent the biological relationships between the nodes. There is an inverse relationship between the length of the edges and the amount of publicly available information about the biologic relationships. Pathway analysis results are displayed in Supplemental Fig. 1.

2.8. Western blot analysis

The following antibodies were used to validate differential protein expression determined by ICAT-LC–MS/MS: β-actin, 1:500 (β-actin from Santa Cruz Biotechnology), serine/threonine–protein kinase, 1:500 (PLK-1 from Zymed Labs), tumor-associated calcium signal transducer 1 precursor, 1:200 (EpCAM from Santa Cruz Biotechnology), T-complex protein 1, beta subunit, 1:200 (TCP-1 β from Santa Cruz Biotechnology), and ribosomal protein S6 kinase alpha 4, 1:200 (Rsk-2 from Santa Cruz Biotechnology). The Rsk-2 antibody detects a closely related protein in the same family as ribosomal protein S6 kinase alpha 4 (RSKB). Forty micrograms of total cell lysate from rituximab-treated cells (10 μg/mL) and untreated cells were separated on 13% discontinuous gels by SDS-PAGE using a mini-PROTEAN II electrophoresis cell (Bio-Rad, Hercules, CA). Proteins were transferred to nitrocellulose membranes (Amersham Biosciences) by semi-dry transfer (Biorad, Hercules, CA). Nitrocellulose membranes were blocked overnight at 4 °C in TTBS plus 5% nonfat milk. Membranes were incubated at room temperature for 1 h in primary antibodies diluted in TTBS plus 5% nonfat milk. Membranes were washed four times for 15 min each followed by a 1 h incubation in horse-radish peroxidase conjugated secondary antibodies (Santa Cruz), also diluted in TTBS plus 5% nonfat milk. Membranes were washed and visualized using enzyme chemiluminescence (Santa Cruz). Western blot band density was measured using ImageMaster TotalLab v.1.11.

2.9. Statistical analysis

Mean values, standard deviations, *t*-tests and *P*-values were calculated using Microsoft Excel.

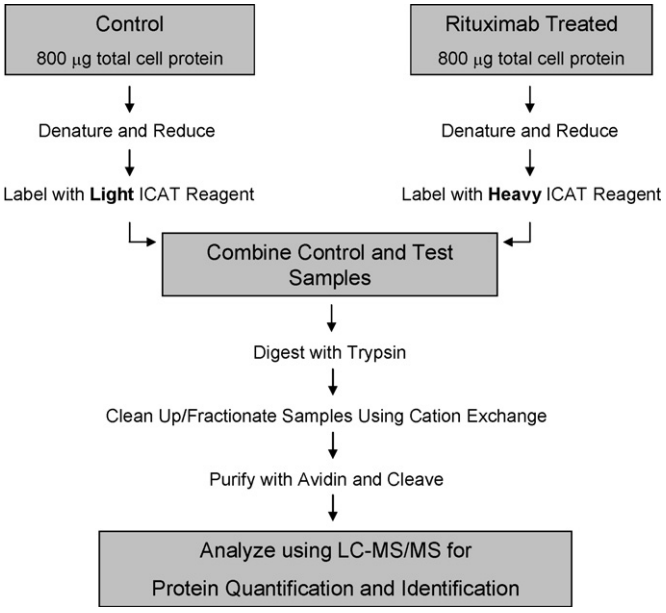

Fig. 2. A schematic overview of the experimental design used for isotope-coded affinity tag labeling, microcapillary liquid chromatography and tandem mass spectrometry. See Section 2 for detailed description.

Table 1
Differentially expressed proteins (>2.0-fold) detected by ICAT.

	Protein accession	Protein description	Num unique peps	ASAP ratio			z	Peptide sequence
				Mean	S.D.	Num peps		
Overexpressed								
1	IPI00012202	Methylosome protein 50	1	18.46	0.32	1	1	ILLWDTRCPK
2	IPI00647363	12 kDa protein	1	12.31	0.41	1	3	RNGAREGGLSLTLGCLSGGR
3	IPI00152661	Polycystic kidney disease 1-like 1 protein	1	6.49	0.21	1	2	KAASDNGTACPAPK
4	IPI00216220	26S proteasome non-ATPase regulatory subunit 9	1	4.96	0.18	1	2	GLLGCNIIPLQR
5	IPI00012283	Semaphorin 3B precursor	1	4.39	0.16	1	2	DIGTECMNFVK
6	IPI00479998	Zinc finger protein 267	1	4.23	0.28	1	2	VFSRSSCLTQHRK
7	IPI00376976	130-kDa phosphatidylinositol 4,5-biphosphate-dependent ARF1 GTPase	2	4.03	0.24	1	2	LKATQCEDLLSQAK
8	IPI00219114	Dynactin1	1	3.91	0.09	1	3	YEHALSQCSVDVYK
9	IPI00001690	Cullin homolog 7	1	3.70	0.16	1	3	CWEKVEVSSNPHR
10	IPI00022367	Astrotactin 1	1	3.41	0.17	1	2	AAGECLCYEGYMK
11	IPI00014137	Oxysterol binding protein-related protein 2	1	3.30	0.09	1	2	CVLHFKPCGLFGK
12	IPI00014835	Mitochondrial ribosomal protein S9	1	3.12	0.21	1	2	LGKHDVTCTVSGGGR
13	IPI00300956	Ribonuclease III	1	3.12	0.17	1	3	HSIYPGEEAIKPCR
14	IPI00022536[a]	**Ribosomal protein S6 kinase alpha 4**	1	2.87	0.28	1	1	ILKCSPPFPPR
15	IPI00304023	Retinoblastoma-binding protein 8	2	2.72	0.24	1	2	ECHDREVQGLQVK
16	IPI00013789	SMYD family member 5	2	2.66	0.05	1	2	PGQVLPHPELCTVR
17	IPI00240598	Semaphorin 6A precursor	1	2.49	0.25	1	2	HKDECHNFIKVLLK
18	IPI00014151	26S proteasome non-ATPase regulatory subunit 6	1	2.46	0.37	1	2	FIAAGRLHCKIDK
19	IPI00413364	43 kDa protein, 59 kDa proteinTBC1 domain family, member 3, TBC1	1	2.41	0.04	1	3	TSRCGPWARFCNRFVDTWAR
20	IPI00550953	Zinc finger protein 20	1	2.37	0.24	1	2	THECKQCGKAFR
21	IPI00021248[a]	**Serine/threonine-protein kinase PLK1**	2	2.29	0.18	1	2	PPFETSCLKETYLR
22	IPI00180730	50 kDa protein, PREDICTED: similar to eukaryotic translation elongation	1	2.27	0.15	1	3	DGNASGTMLLEALDCILPPTRPTDK
23	IPI00103563	Ankyrin repeat and SOCSbox containing protein 15	1	2.12	0.41	1	2	VLIDYMDYVPLCAK
24	IPI00030997	ForkheadboxproteinG1C	1	2.11	0.23	1	2	DNLSLNKCFVKVPR
25	IPI00216028	Ankyrin repeat and SOCSbox containing protein2	2	2.01	0.10	2	2	AEPPRPLAHLCRLR
Underexpressed								
1	IPI00396057	Chromosome 9 open reading frame 10, Splice Isoform A of Protein C9o	1	0.11	0.01	1	2	VAAASGHCGAFSGSDSSR
2	IPI00162088	TNF receptor-associated factor 4	1	0.18	0.27	1	1	TQPCTYCTK
3	IPI00386371	Seven transmembrane helix receptor	2	0.19	0.05	1	3	AASCLLRYTTSELRGCYGSLK
4	IPI00386763	ADAMTS-9 precursor	1	0.19	0.11	1	3	NDVLDDSKCTHQEK
5	IPI00296215[a]	**Tumor-associated calcium signal transducer 1 precursor**	1	0.23	0.09	1	1	DTEITCSERVR
6	IPI00456244	Centaurin gamma 2	1	0.24	0.12	1	2	DEVNETCGEGDGR
7	IPI00386697	ADAMTS-16 precursor	2	0.25	0.11	2	2	LCMLDFKKDICK
8	IPI00399320	Protein C1 orf8 precursor	1	0.29	0.19	1	2	ACQLTYPLHTYPK
9	IPI00297779[a]	**T-complex protein 1, beta subunit**	1	0.30	0.08	1	2	SLHDALCVLAQTVK
10	IPI00030116	Phosphoacetylglucosamine mutase	1	0.33	0.26	1	3	GKLNHLCGADFVK
11	IPI00220818	Zinc finger protein PL AGL1	1	0.34	0.07	1	2	DFLCQFCAQRFGRK
12	IPI00646638	23 kDa protein	2	0.34	0.08	1	3	VCEKALDSSSFLQRHKRTHTGEK
13	IPI00028464	Kelch-like protein4	1	0.34	0.06	1	2	LYAIGGRDGSSCLK
14	IPI00218130	Glycogen phosphorylase, muscle form	1	0.35	0.14	1	2	VFADYEDYIKCQEK
15	IPI00029658	EGF-containing fibulin-like extracellular matrix protein 1 precursor	2	0.36	0.21	2	2	NPCQDPYILTPENR
16	IPI00220349	Eukaryotic translation initiation factor 2C 2	2	0.37	0.20	2	2	HHTRLFCTDKNER
17	IPI00023234	Ubiquitin-like 2 activating enzyme E1B	1	0.43	0.08	1	2	NTPSEPIHCIVWAK
18	IPI00003027	Gem-associated protein 7	1	0.46	0.09	1	1	CSDIISYTFKP
19	IPI00029045	Inhibitor of nuclear factor kappa-B kinase epsilon subunit	1	0.47	0.09	1	2	RLLQVFQEECVQK

[a] Proteins in bold were confirmed by immunoblot analysis.

3. Results

3.1. Rituximab decreases cell viability of SUDHL-4 cells

The SUDHL-4 B-cell lymphoma-derived cell line was used based on previous reports demonstrating its susceptibility to rituximab [10]. Viability assays were performed to determine the optimal concentration and time point for subsequent mass spectrometric experiments. Cells were incubated with increasing concentrations of rituximab (10, 20, and 50 μg/mL) or without the drug (media control) for several time points (24, 48, 72, and 96 h). As shown in Fig. 1A, rituximab (10 μg/mL) decreased cell viability by 86.1% at 24 h, 65.7% at 48 h, 49.8% at 72 h, and 46.5% at 96 h ($n = 3$). A dose-dependent effect on viability was not observed. As shown in Fig. 1B, at a time point of 48 h, rituximab reduced cell viability by 71.7% at 10 μg/mL, 76.1% at 20 μg/mL, and 58.2% at 50 μg/mL ($n = 3$). Based on these experiments a concentration of 10 μg/mL and a time point of 48 h were used for subsequent ICAT–LC–MS/MS analysis. To confirm rituximab's effect at 10 μg/mL for 48 h, we repeated the viability assay in 18 independent experiments which demonstrated that rituximab decreased the viability by 31.2 ± 2.9% compared to the media control ($P < 0.0001$) (data not shown).

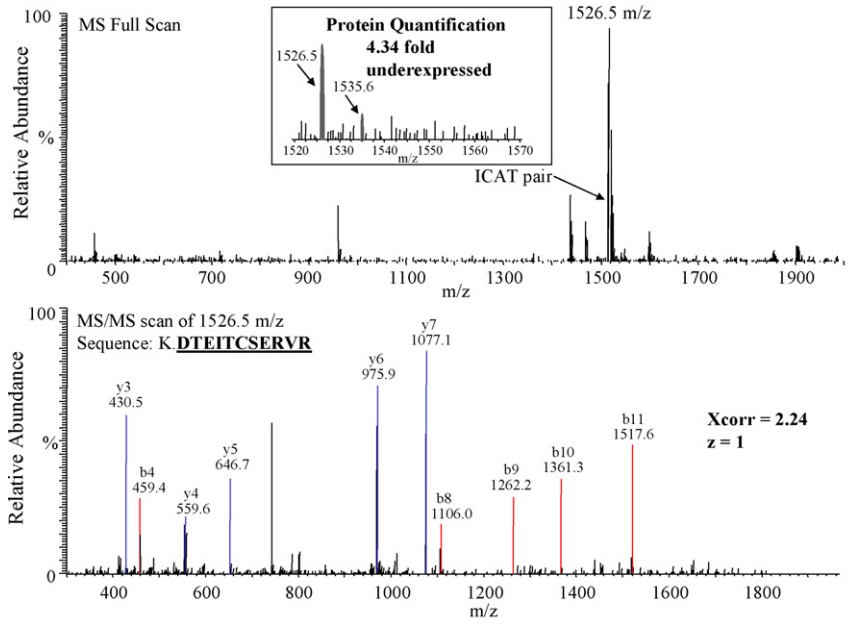

	AA	B ions	Y ions	
1	D	116.09	1535.56	11
2	T	217.20	1420.47	10
3	E	346.31	1319.37	9
4	I	459.47	1190.25	8
5	T	560.58	1077.09	7
6	C	879.85	975.99	6
7	S	976.92	646.72	5
8	E	1106.04	559.64	4
9	R	1262.23	430.53	3
10	V	1361.36	274.34	2
11	R	1517.55	175.21	1

PROTEIN: TTD1_HUMAN (P16422) Tumor-associated calcium signal transducer 1 (EpCAM)

MAPPQVLAFGLLLAAATATFAAAQEECVCENYKLAVNCFVNNNRQCQCTSVGAQNTVICSKLAAKCLVMKAEMNGSKL
GRRAKPEGALQNNDGLYDPDCDESGLFKAKQCNGTSTCWCVNTAGVRRTDK**DTEITCSERVR**TYWIIIELKHKAREKPY
DSKSLRTALQKEITTRYQLDPKFITSILYENNVITIDLVQNSSQKTQNDVDIADVAYYFEKDVKGESLFHSKKMDLTVNGEQ
LDLDPGQTLIYYVDEKAPEFSMQGLKAGVIAVIVVVVMAVVAGIVVLVISRKKRMAKYEKAEIKEMGEMHRELNA

Fig. 3. MS full scan and data-dependent MS/MS scan showing sequencing of the ICAT tryptic peptide K.DTEITCSERVR which identified EpCAM as underexpressed 4.34-fold. Peptide sequencing is indicated by matching b ion (red) and y ion (blue) fragments.

3.2. Rituximab induces caspase-3 activity

There have been reports of rituximab acting on both caspase-dependent and independent pathways to initiate apoptosis [11–16]. We used a caspase-3 activity assay to assess the activation of caspase by rituximab in SUDHL-4 cells. As shown in Fig. 1C, rituximab caused an increase in caspase-3 activity by 1.7-fold compared to the media control ($n = 2$). Caspase-3 activity was abrogated by the presence of the caspase inhibitor Z-VAD FMK.

3.3. Rituximab does not induce cell cycle arrest

We used flow cytometry to determine the effect of rituximab on cell cycle parameters. Rituximab did not affect the cell cycle parameters. Total S phase cells were 47.16% with rituximab treatment and 47.36% for control. Total G_1 phase cells were 38.78% in treated cells and 38.57% in untreated cells. Total G_2 phase cells were 14.06% in treated cells and 14.08% in untreated cells. The hypodiploid peak, however, was increased in treated cells by 4.91%, indicating a small increase in apoptotic cells (data not shown).

3.4. ICAT identifies differentially expressed proteins in rituximab-treated cells

Isotope-coded affinity tag (ICAT) analysis was used to evaluate global protein expression changes in response to rituximab. The experimental overview is shown in Fig. 2. Protein from total cell lysates was digested with trypsin and labeled with heavy and light cleavable ICAT reagent. The combined ICAT-labeled peptides were fractionated using strong cation exchange, purified using avidin affinity chromatography, separated using microcapillary chromatography and subjected to electrospray ionization. Tandem mass spectrometry identified the proteins and determined the relative abundance using heavy and light ICAT reagents [17]. A total of 92 proteins were found to be differentially expressed, of which 44 proteins were differentially expressed by greater than 2.0-fold in the rituximab-treated cells compared to the media control. Twenty-five of these were upregulated, and 19 were downregulated. Table 1 summarizes the differentially expressed proteins according to magnitude, with selected proteins confirmed by western blot analysis highlighted in bold text. Fig. 3 shows the relative quantification and identification of tumor-associated calcium signal transducer 1 precursor (EpCAM), while Xpress integration of light and heavy peptides is detailed for EpCAM in Fig. 4. Several functional groups were identified within the differentially expressed proteins, including membrane proteins (olfactory receptor, integrin alpha-7 precursor, seven transmembrane helix receptor), transcription factors (forkhead box protein G1C, zinc finger proteins 20, 267 and 445), proteins involved in migration and adhesion (astrotactin 1 and T-complex protein 1, beta subunit), proteins associated with the ubiquitin–proteasome (cullin homolog 7, 26S proteasome non-ATPase regulatory subunit 9), proteins affecting calcium-induced

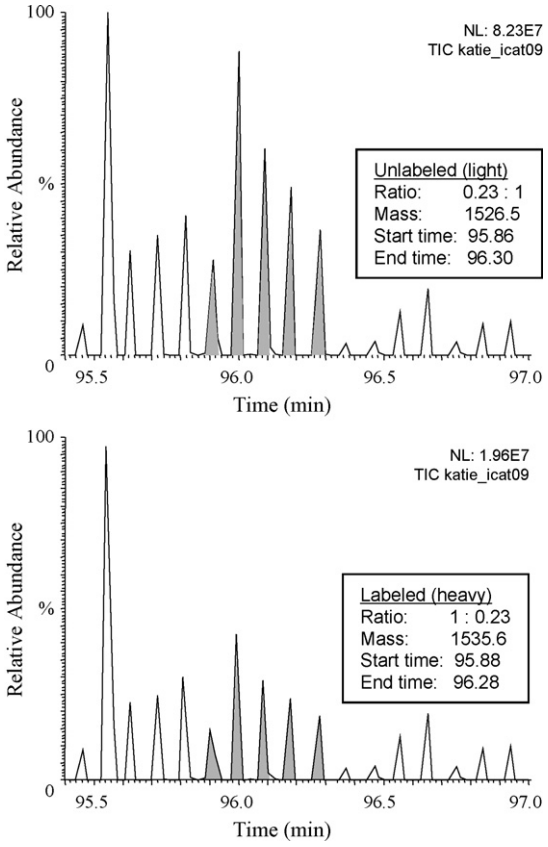

Fig. 4. Details of Xpress quantitation for EpCAM showing integration of the heavy and light peptide at 1.00:0.23 (4.34 underexpressed).

signaling (tumor-associated calcium signal transducer 1 precursor), and components of the phosphoinositol (phosphatidylinositol 4-kinase alpha) and NF-κB pathways (inhibitor of nuclear factor kappa-B kinase epsilon subunit and TRAF4). Table 2 summarizes the putative molecular functional groups according to the NCBI-conserved domain database.

Notably, some proteins corroborate with previously proposed mechanisms of action of rituximab, including signaling through lipid rafts (130-kDa PIP2-dependent ARF1 GTPase activating protein, phosphatidylinositol 4-kinase alpha) [18,19], calcium influx (130-kDa PIP2-dependent ARF1 GTPase activating protein, tumor-associated calcium signal transducer 1 precursor, phosphatidylinositol 4-kinase alpha) [14], and the NF-kB pathways (inhibitor of nuclear factor kappa-B kinase epsilon subunit and TRAF4) [20,21]. The categorization of differentially expressed proteins into functional groups according to the GO MINER database is illustrated in Fig. 5A. The results highlight that for both up and downregulated proteins, those that perform catalytic, binding and signaling functions make up the largest groups. Furthermore, classification of the proteins according to cellular localization (Fig. 5B), suggests that the effects of rituximab occur throughout all compartments of the cell.

Several important proteins shown to affect cell viability in other studies (semaphorin 3B precursor, polo-like kinase 1) but not previously implicated in rituximab pathways were also identified. Interestingly, several differentially expressed proteins (polycystic kidney disease 1-like protein, semaphorin3B, ADAMTS, astrotactin 1) have not previously been reported to be expressed in lymphocytes.

3.5. Western blots validate ICAT data

We verified differential expression of selected proteins by western blot analysis. Fig. 6 shows the differential expression of tumor-associated calcium signal transducer 1 precursor (EpCAM), T-complex protein 1, beta subunit (TCP-1 β), serine/threonine-protein kinase (PLK-1), and ribosomal protein S6 kinase alpha 4 (Rsk-2 is a protein in the same family as ribosomal protein S6 kinase alpha 4) with corresponding ICAT ratios. Actin was used as a loading control. Densitometric analysis of the western blots for EpCAM and TCP-1 β demonstrated that they were downregulated by 0.76- and 0.81-fold, respectively, while ICAT data demonstrated downregulation by 0.23 and 0.30. PLK-1 and Rsk-2 were upregulated by 1.95- and 1.67-fold, respectively, while ICAT demonstrated upregulation by 2.29 and 2.87. Although the densitometry measurements did not match the measured ICAT differential expression exactly, there was general concordance in up- or downregulation of proteins.

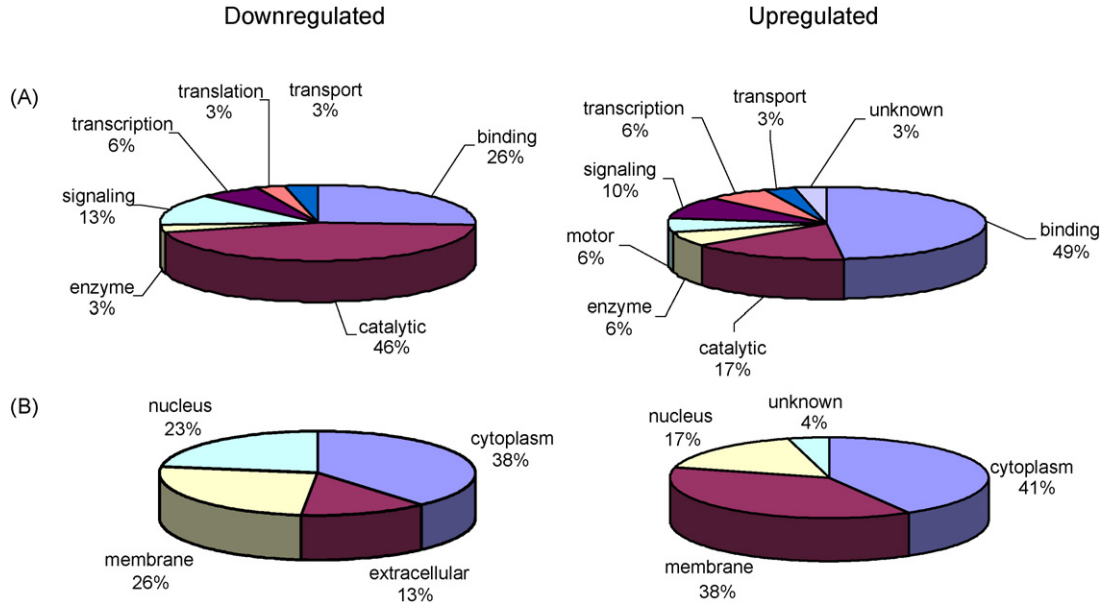

Fig. 5. Classification of differentially expressed proteins according to (A) functional groups and (B) cellular localization using GOMiner.

Table 2
categories of molecular function for differentially expressed proteins (>2.0-fold).

IPI accession	Protein description	ASAP ratio	Protein function[a]
Apoptosis regulation			
IPI00012283	Semaphorin 3B precursor	4.39	Sema, PSI
IPI00013481	Baculoviral IAP repeat-containing protein 2	0.54	BIR, CARD, RING
Cell cycle			
IPI00304023	Retinoblastoma-binding protein 8	2.72	CTBP
IPI00023234	Ubiquitin-like 2 activating enzyme ElB	0.43	Uba2_SUMA, El-2_like
Cell growth			
IPI00216028	Ankyrin repeat and SOCS box containing protein 2	2.01	ANK, SOCS
IPI00296215	Tumor-associated calcium signal transducer 1 precursor	0.23	TY
Cell signaling			
IPI00376976	130-kDa phosphatidylinositol 4,5-biphosphate-dependent ARF1 GTPase-activating protein	4.03	PH, ANK, SH3, ArfGAP
IPI00014137	Oxysterol binding protein-related protein 2	3.30	Oxysterol_BP
IPI00022536	Ribosomal protein S6 kinase alpha 4	2.87	S_TKc, TyrKc
IPI00456244	Centaurin gamma 2	0.24	PH, RAB, ANK, ArfGap
Extracellular matrix			
IPI00386697	ADAMTS-16 precursor	0.25	ADAM, TSpl, Reprolysin
IPI00029658	EGF-containing fibulin-like extracellular matrix protein 1 precursor	0.21	vWA_Matrillin, EGF_CA
IPI00386763	ADAMTS-9 precursor	0.19	ADAM, TSpl, Reprolysin
Migration/adhesion			
IPI0022367	Astrotactin 1	3.41	MACPE
IPI0028464	Kelch-like protein 4	0.34	BTB, Kelch
IPI000297779	T-complex protein 1, beta subunit	0.30	Cpn60_TCP1, GroL
Membrane-associated proteins			
IPI00399320	Protein C1orf8 precursor	0.29	ABC_ATPase, ABC_tran
IPI00386371	Seven transmembrane helix receptor	0.19	7tm_1, cyclin_like
Metabolism			
IPI00218130	Glycogen phosphorylase, muscle from	0.35	Phosphorylase, GlgP
IPI00030116	Phosphoacetylglucosamine mutase	0.33	PGM_PMM_I, ManB
NF-κB			
IPI00029045	Inhibitor of nuclear factor kappa-B kinase epsilon subunit	0.47	S_TKc, TyrKc, SPS1
IPI00162088	TNF receptor-associated factor 4	0.18	RING, zf-TRAF, MATH
Protein synthesis/degradation			
IPI00216220	26S proteasome non-ATPase regulatory subunit 9	4.96	PDZ_metalloprotese, DegQ
IPI00001690	Cullin homolog 7	3.70	Cullin, APC10, DOC1
IPI00300956	Ribonuclease III	3.12	RIBOc, DSRM, Rnc
IPI00220349	Eukaryotic translation ignition factor 4	0.37	PAZ, Piwi
SMN complex/small nuclear ribonucleoproteins			
IPI00012202	Methylosome protein 50	18.46	WD40
IPI00003027	Gem-associated protein 7	0.46	
Transcription factors			
IPI00479998	Zinc finger protein 267	4.23	KRAB, Zn-finger
IPI00030997	Frokhead box protein GIC	2.11	Forkhead
IPI00220808	Zinc finger protein PLAGL1	0.34	z-fC2H2

[a] NCBI conserved domains results from http://www.ncbi.nlm.nih.gov/Stucture/cdd/cdd.shtml.

3.6. Pathway analysis

We analyzed the differentially expressed proteins using a web-based program (Ingenuity Pathway Analysis). Proteins identified in the ICAT analysis highlighted prominent signaling pathways including apoptosis, B-cell signaling, cell cycle regulation, integrin signaling, and the NF-κB signaling pathway (Supplemental Fig. 1). In addition, many of the ICAT identified proteins did not belong to well-characterized pathways suggesting that rituximab may affect novel, previously uncharacterized pathways.

4. Discussion

This is the first report in which quantitative proteomic analysis has been used to evaluate differential protein expression in neoplastic B-cells after rituximab exposure. ICAT in conjunction with microcapillary liquid chromatography and tandem mass spectrometry (LC–MS/MS), have provided a novel way to identify and quantify global protein expression patterns in different cellular states or tissues [4,22]. Separate protein pools are digested and cysteine-containing peptides labeled with heavy or light ICAT reagents. Tagging different peptide pools assumes that the same proteins, with different labels, will behave identically during isolation, separation and ionisation [4]. Three-dimensional separation, using strong cation exchange/avidin affinity/reversed phase column separations achieves improved chromatographic resolution and identification of lower abundance proteins [17]. Analysis of the labeled peptides by tandem mass spectrometry can then provide both relative quantitation and identification of proteins in the sample. Our current ICAT–LC–MS/MS analysis of lymphoma-derived cells exposed to rituximab demonstrates important changes in many proteins including those involved in migration and adhesion, signaling pathways, apoptosis, transcription regulation, and protein synthesis and degradation.

The differentially expressed proteins included semaphorin 3B precursor (SEMA3B), which was upregulated by 4.39-fold in

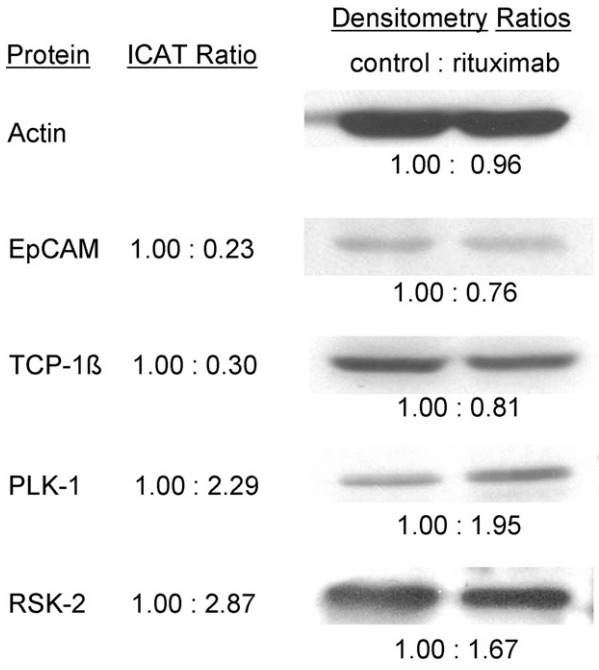

Fig. 6. Western blot analysis of protein expression changes induced by rituximab. Antibodies were used to verify selected protein identification by MS/MS; tumor-associated calcium signal transducer 1 precursor (EpCAM), polo-like kinase 1 (PLK-1), T-complex protein 1, beta subunit (TCP-1ß), and ribosomal protein S6 kinase alpha 4 (RSK-2). Actin was the loading control. The density of the bands was measured using ImageMaster TotalLab v.1.11, and compared to that in the media control treated cells, which was set at 1.0. The ICAT ratios of the up- and downregulated proteins are shown for comparison.

rituximab-treated cells. SEMA3B plays a role in axonal guidance in developing brain tissue and has also been shown to have pro-apoptotic properties in breast and lung cancer [23–25]. While the significance of expression of SEMA3B in normal and neoplastic lymphoid cells is unknown, the upregulation of this protein in rituximab-treated cells suggests that it may mediate the pro-apoptotic effect of rituximab in lymphocytes.

Similarly, the 130-kDa PIP2-dependent ARF1 GTPase activating protein (ASAP1/DEF-1) was upregulated by 4.03-fold in rituximab-treated cells. This protein binds to both PIP_2 and Src and is a substrate of Src tyrosine kinase [26–28]. ASAP1/DEF1 plays a role in focal adhesion assembly and PDGF-induced membrane ruffling [26–29] and regulates cell spreading and motility. Transient overexpression of ASAP1/DEF-1 decreased cell spreading via the prevention of organization of paxillin and FAK, while stable expression of ASAP1/DEF-1 enhanced cell migration [27]. Although there is no biochemical data to support the idea that rituximab alters cellular morphology or invasive or migratory properties, the upregulation of ASAP1/DEF-1 by rituximab may result in deregulation of cell spreading or membrane ruffling. Alternatively, it may assist in Src and PIP_2 mediated signaling. Activation of Src-family tyrosine kinases has been suggested as a key function in lipid raft facilitated signaling, and signaling events caused by rituximab have been blocked using PP2, a selective inhibitor of Src-family kinases [16]. Other studies suggest that lipid rafts are enriched in Src-family tyrosine kinases, so that the binding of rituximab to CD20 associated with lipid rafts trans-activates the kinases and initiates downstream signaling to promote apoptosis [19]. Upregulation of this protein may also assist in Src-family tyrosine kinase signaling that is detrimental to cell viability.

Polo-like kinase 1 (PLK-1) was upregulated by 2.29-fold. PLK-1 is involved in cell cycle checkpoint progression, and is critical for successful completion of mitosis [30]. Cells with damaged DNA are dependent on PLK-1 degradation of Wee-1 for recovery [31]. The upregulation of PLK-1 suggests general derangement of the mitotic machinery in rituximab-treated cells.

The ribosomal protein S6 kinase alpha 4/mitogen-and stress-activated protein kinase-2 (RSKB/MSK2) was upregulated by 2.87-fold in rituximab-treated cells. RSKB/MSK2 is a substrate for p38αMAPK and ERKs [32,33]. It phosphorylates cAMP response element-binding protein (CREB) and activating transcription factor-1 (ATF1), and plays a role in transcription of COX-2 and IL-1β genes when macrophages are stimulated by lipopolysaccharide, making RSKB/MSK2 a possible anti-inflammatory target [33]. It has been hypothesized that rituximab interferes with the ERK1/2 pathway, which in turn leads to the downregulation of Bcl-x_L, an anti-apoptotic protein [34,35]. Other studies have shown conflicting information on rituximab's effect on p38 MAPK. One study on B-CLL cells suggested that rituximab, when crosslinked, induced sustained phosphorylation of p38 MAPK, ERK, and JNK, while an inhibitor of p38 MAPK decreased rituximab's apoptotic effect [36]. In another study using 2F7 cells which were resistant to the cytotoxic effect of rituximab, the p38 MAPK pathway was inhibited by rituximab [37]. The conflicting data may reflect cell-type specific responses. The upregulation of RSKB/MSK2 seen in our experiment suggests that rituximab may induce apoptosis via p38 MAPK activation consistent with previous observations [36].

The TNF receptor-associated factor 4 (TRAF4) was downregulated by 0.18 in rituximab-treated SUDHL-4 cells. Members of the tumor necrosis factor receptor family such as TRAF4 function as adaptor molecules in several signaling pathways, including the NF-κB and JNK pathways [38]. One study indicates that TRAF4 augments NF-κB pathway activation when it is triggered by a glucocorticoid-induced tumor necrosis factor receptor (GITR) found on B-cells, T cells and macrophages [39]. Another study suggested that TRAF4 transcription in T cells and Jurkat cells is greatly increased when NF-κB is induced by TNF, and decreased when essential components of the NF-κB activation complex are missing [21]. TRAF4 has also been found to be a binding partner for p70S6K, a serine/threonine kinase involved in cell cycle progression, and may inhibit Fas-induced apoptosis [40]. The downregulation of TRAF4 seen by our ICAT experiment would be consistent with a decrease in NF-κB activation and a decrease in activity of p70S6K, resulting in a decrease in cell cycle progression and decreased cell viability. The downregulation of NF-κB and other components of the pathway by rituximab have been observed in a recent study [41]. Importantly, the role of TRAF4 in mediating the inhibition of NF-κB has not been previously reported and implicates it in the pathogenesis of B-cell lymphoproliferative disorders.

The inhibitor of nuclear factor kappa-B kinase epsilon subunit (IKKE) was downregulated 0.47-fold. IKKE phosphorylates inhibitors of NF-κB, leading to degradation of the inhibitors and activation of NF-κB [20]. IKKE downregulation caused by rituximab will ultimately lead to a decrease in NF-κB activity, which may decrease cell viability. IKKE is also a component of the interferon regulatory factor 3 (IRF3) pathway. IRF3 and NF-κB are important in the innate immune response, promoting cell death in virally infected cells and giving healthy cells protection using interferons [42]. The downregulation of IKKE was expected, as another source has shown that NF-κB activity is decreased, and subsequently anti-apoptotic Bcl-x_L is downregulated, in lymphoma cells treated with rituximab [41].

The tumor-associated calcium signal transducer 1 precursor (EpCAM) was downregulated 0.23-fold. EpCAM is a regulator of cell adhesion and is overexpressed in breast cancer, colon cancer and retinoblastoma [43,44]. It is also implicated in the regulation of cell proliferation and adhesion by enhancing E-cadherin-mediated

cell-to-cell adhesion in breast cancer [43]. EpCAM is also thought to induce cell proliferation by the upregulation of the Myc oncogene [45]. The expression of EpCAM in lymphocytes has not been previously reported and may play a role in the growth and adhesive properties of lymphoma cells.

The phosphatidylinositol 4-kinase alpha protein (PI4-Kα) was downregulated 0.61-fold (Supplemental Table 1). This protein is important for cell viability. It acts on phosphatidylinositol during the first committed step to IP_3 production [46]. The IP_3 receptor is a key intracellular calcium release channel that responds to many signals, and it regulates diverse functions including contraction, excitation, gene expression and cellular growth [47]. It has also been shown that the protein family of tetraspanin proteins that includes PI4-Kα localize into microdomains resembling lipid rafts [48]. Lipid raft reorganization and signaling has been implicated in rituximab action [18]. Lipid rafts serve as platforms for signal transduction and organization [19]. Rituximab may redistribute CD20 receptors into lipid rafts to activate Src-family tyrosine protein kinases and allow calcium influx, eventually activating caspase 3 [16]. The downregulation of lipid raft associated PI4-Kα may affect cell viability by decreasing levels of IP_3, and therefore cell growth and migration.

Several identified proteins have not been previously reported to be expressed in lymphocytes (polycystic kidney disease 1-like protein, ADAMTS, astrotactin 1). Additionally, our data suggest that proteins involved in metabolic machinery, ubiquitin/proteasome machinery, adhesion, migration, invasion, endocytosis, nuclear transport and protein synthesis are affected by rituximab. Pathway analysis illustrates some of the major proteins and corresponding pathways that are affected by rituximab (Supplemental Fig. 1).

Techniques such as microarray or tag-based gene expression analysis and genome wide association studies (GWAS) are commonly used to study large-scale gene expression patterns. Expression array data sets have been generated for many types of disease associations including cancer. Expression profiling has also been performed for rituximab treatment in B-cell follicular lymphoma [49]. Software tools such as Gene Set Enrichment Analysis and Oncomine are useful when analyzing large gene expression data sets [50,51]. Further investigation will be necessary to correlate the proteome response of rituximab treatment to gene expression profiles in B-cell lymphoma.

In conclusion, we have used a global quantitative proteomic approach to evaluate the intracellular proteomic changes that occur in B-cell lymphomas as a result of rituximab treatment.

Our results indicate that rituximab induced the differential expression of many proteins important in diverse cellular functions including integral membrane proteins, proteins involved in migration and adhesion, proteins affecting calcium-induced signaling, proteins associated with the cell cycle, and components of the phosphoinositol and NF-κB pathways. Our results highlight the utility of quantitative LC–MS/MS in the discovery of broad cellular consequences in response to therapeutic monoclonal antibody.

Acknowledgement

This work was supported by ARUP Institute for Clinical and Experimental Pathology™.

Appendix A. Supplementary data

Supplementary data associated with this article can be found, in the online version, at doi:10.1016/j.jchromb.2008.10.036.

References

[1] M.R. Loken, V.O. Shah, Z. Hollander, C.I. Civin, Pathol. Immunopathol. Res. 7 (1988) 357.
[2] W. Rastetter, A. Molina, C.A. White, Annu. Rev. Med. 55 (2004) 477.
[3] D.G. Maloney, Curr. Hematol. Rep. 2 (2003) 13.
[4] S.P. Gygi, B. Rist, S.A. Gerber, F. Turecek, M.H. Gelb, R. Aebersold, Nat. Biotechnol. 17 (1999) 994.
[5] P.J. Kersey, J. Duarte, A. Williams, Y. Karavidopoulou, E. Birney, R. Apweiler, Proteomics 4 (2004) 1985.
[6] J. Peng, J.E. Elias, C.C. Thoreen, L.J. Licklider, S.P. Gygi, J. Proteome Res. 2 (2003) 43.
[7] X.J. Li, H. Zhang, J.A. Ranish, R. Aebersold, Anal. Chem. 75 (2003) 6648.
[8] A. Keller, A.I. Nesvizhskii, E. Kolker, R. Aebersold, Anal. Chem. 74 (2002) 5383.
[9] A.I. Nesvizhskii, A. Keller, E. Kolker, R. Aebersold, Anal. Chem. 75 (2003) 4646.
[10] N. Di Gaetano, Y. Xiao, E. Erba, R. Bassan, A. Rambaldi, J. Golay, M. Introna, Br. J. Haematol. 114 (2001) 800.
[11] H.T. Chan, D. Hughes, R.R. French, A.L. Tutt, C.A. Walshe, J.L. Teeling, M.J. Glennie, M.S. Cragg, Cancer Res. 63 (2003) 5480.
[12] M. Stanglmaier, S. Reis, M. Hallek, Ann. Hematol. 83 (2004) 634.
[13] L.E. van der Kolk, L.M. Evers, C. Omene, S.M. Lens, S. Lederman, R.A. van Lier, M.H. van Oers, E. Eldering, Leukemia 16 (2002 1735).
[14] D. Shan, J.A. Ledbetter, O.W. Press, Cancer Immunol. Immunother. 48 (2000) 673.
[15] J.C. Byrd, S. Kitada, I.W. Flinn, J.L. Aron, M. Pearson, D. Lucas, J.C. Reed, Blood 99 (2002 1038).
[16] J.K. Hofmeister, D. Cooney, K.M. Coggeshall, Blood Cells Mol. Dis. 26 (2000) 133.
[17] R. Aebersold, M. Mann, Nature 422 (2003) 198.
[18] I. Semac, C. Palomba, K. Kulangara, N. Klages, G. van Echten-Deckert, B. Borisch, D.C. Hoessli, Cancer Res. 63 (2003) 534.
[19] J.P. Deans, H. Li, M.J. Polyak, Immunology 107 (2002) 176.
[20] R.T. Peters, S.M. Liao, T. Maniatis, Mol. Cell 5 (2000) 513.
[21] H. Glauner, D. Siegmund, H. Motejadded, P. Scheurich, F. Henkler, O. Janssen, H. Wajant, Eur. J. Biochem. 269 (2002) 4819.
[22] R. Aebersold, D.R. Goodlett, Chem. Rev. 101 (2001) 269.
[23] E. Castro-Rivera, S. Ran, P. Thorpe, J.D. Minna, Proc. Natl. Acad. Sci. U. S. A. 101 (2004) 11432.
[24] Y. Sekido, S. Bader, F. Latif, J.Y. Chen, F.M. Duh, M.H. Wei, J.P. Albanesi, C.C. Lee, M.I. Lerman, J.D. Minna, Proc. Natl. Acad. Sci. U. S. A. 93 (1996) 4120.
[25] C. Tse, R.H. Xiang, T. Bracht, S.L. Naylor, Cancer Res. 62 (2002) 542.
[26] M.T. Brown, J. Andrade, H. Radhakrishna, J.G. Donaldson, J.A. Cooper, P.A. Randazzo, Mol. Cell. Biol. 18 (1998) 7038.
[27] Y. Liu, J.C. Loijens, K.H. Martin, A.V. Karginov, J.T. Parsons, Mol Biol. Cell 13 (2002) 2147.
[28] P.A. Randazzo, J. Andrade, K. Miura, M.T. Brown, Y.Q. Long, S. Stauffer, P. Roller, J.A. Cooper, Proc. Natl. Acad. Sci. U. S. A. 97 (2000) 4011.
[29] C. Furman, S.M. Short, R.R. Subramanian, B.R. Zetter, T.M. Roberts, J. Biol. Chem. 277 (2002) 7962.
[30] I. Sumara, J.F. Gimenez-Abian, D. Gerlich, T. Hirota, C. Kraft, C. de la Torre, J. Ellenberg, J.M. Peters, Curr. Biol. 14 (2004 1712).
[31] M.A. van Vugt, A. Bras, R.H. Medema, Mol. Cell 15 (2004) 799.
[32] B. Pierrat, J.S. Correia, J.L. Mary, M. Tomas-Zuber, W. Lesslauer, J. Biol. Chem. 273 (1998) 29661.
[33] M. Caivano, P. Cohen, J. Immunol. 164 (2000) 3018.
[34] A.R. Jazirehi, M.I. Vega, D. Chatterjee, L. Goodglick, B. Bonavida, Cancer Res. 64 (2004) 7117.
[35] A.R. Jazirehi, X.H. Gan, S. De Vos, C. Emmanouilides, B. Bonavida, Mol. Cancer Ther. 2 (2003) 1183.
[36] I.M. Pedersen, A.M. Buhl, P. Klausen, C.H. Geisler, J. Jurlander, Blood 99 (2002) 1314.
[37] M.I. Vega, S. Huerta-Yepaz, H. Garban, A. Jazirehi, C. Emmanouilides, B. Bonavida, Oncogene 23 (2004) 3530.
[38] J.R. Bradley, J.S. Pober, Oncogene 20 (2001) 6482.
[39] E.M. Esparza, R.H. Arch, Cell. Mol. Life Sci. 61 (2004) 3087.
[40] D.S. Fleckenstein, W.G. Dirks, H.G. Drexler, H. Quentmeier, Leuk. Res. 27 (2003) 687.
[41] A.R. Jazirehi, S. Huerta-Yepez, G. Cheng, B. Bonavida, Cancer Res. 65 (2005) 264.
[42] K.A. Fitzgerald, S.M. McWhirter, K.L. Faia, D.C. Rowe, E. Latz, D.T. Golenbock, A.J. Coyle, S.M. Liao, T. Maniatis, Nat. Immunol. 4 (2003) 491.
[43] W.A. Osta, Y. Chen, K. Mikhitarian, M. Mitas, M. Salem, Y.A. Hannun, D.J. Cole, W.E. Gillanders, Cancer Res. 64 (2004) 5818.
[44] S. Krishnakumar, A. Mohan, K. Mallikarjuna, N. Venkatesan, J. Biswas, M.P. Shanmugam, L. Ren-Heidenreich, Invest. Ophthalmol. Vis. Sci. 45 (2004) 4247.
[45] M. Munz, C. Kieu, B. Mack, B. Schmitt, R. Zeidler, O. Gires, Oncogene 23 (2004) 5748.
[46] K. Wong, L.C. Cantley, J. Biol. Chem. 269 (1994) 28878.
[47] R.L. Patterson, D. Boehning, S.H. Snyder, Annu. Rev. Biochem. 73 (2004) 437.
[48] C. Claas, C.S. Stipp, M.E. Hemler, J. Biol. Chem. 276 (2001) 7974.
[49] S.P. Bohen, O.G. Troyanskaya, O. Alter, R. Warnke, D. Botstein, P.O. Brown, R. Levy, Proc. Natl. Acad. Sci. U. S. A. 100 (2003 1926).
[50] A. Subramanian, P. Tamayo, V.K. Mootha, S. Mukherjee, B.L. Ebert, M.A. Gillette, A. Paulovich, S.L. Pomeroy, T.R. Golub, E.S. Lander, J.P. Mesirov, Proc. Natl. Acad. Sci. U. S. A. 102 (2005) 15545.
[51] D.R. Rhodes, J. Yu, K. Shanker, N. Deshpande, R. Varambally, D. Ghosh, T. Barrette, A. Pandey, A.M. Chinnaiyan, Neoplasia 6 (2004) 1.